In vivo optical reflectance imaging of spreading depression waves in rat brain with and without focal cerebral ischemia

Shangbin Chen
Zhe Feng
Pengcheng Li
Huazhong University of Science and Technology
Key Laboratory of Biomedical Photonics of Ministry of Education
Hubei Bioinformatics and Molecular Imaging Key Laboratory
Wuhan 430074, China

Steven L. Jacques
Oregon Health and Science University
Dermatology and Biomedical Engineering
3181 Southwest Sam Jackson Park Road
Portland, Oregon 97239

Shaoqun Zeng
Qingming Luo
Huazhong University of Science and Technology
Key Laboratory of Biomedical Photonics of Ministry of Education
Hubei Bioinformatics and Molecular Imaging Key Laboratory
Wuhan 430074, China
E-mail: qluo@mail.hust.edu.cn

Abstract. Spreading depression (SD) waves occur in focal cerebral ischemia of the brain. Optical reflectance imaging at 550±10-nm wavelength using a charge-coupled device (CCD) camera, called optical intrinsic signal imaging (OISI) in the neuroscience community, provides high resolution imaging of SD waves based on changes in blood perfusion. We present optical images of SD waves in normal rat brain induced by a pinprick, and the spontaneous SD waves that follow middle cerebral artery occlusion (MCAO). The images of change in reflectance are calculated as $A=(I-I_o)/I_o$, where I is pixel intensity as some timepoint and I_o is the initial intensity just prior to an SD wave. Difference images $B=[I(i)-I(i-1)]/I_o$, where $I(i)$ is the image at time i and $I(i-1)$ is the previous image at time $i-1$ (a 6.4-s interval), significantly sharpen the boundaries between leading and trailing edges of the SD wave. Maximum rate-of-change images $C=\max(B)$ display the maximum pixel value of B within the duration of a single SD wave, and provide an image that visualizes the entire penumbra. The penumbra appear bright due to a rapid drop in perfusion, while the normal brain and infarct area appear dark. [DOI: 10.1117/1.2203654]

Keywords: focal cerebral ischemia; middle cerebral artery occlusion; optical intrinsic signal imaging; spreading depression.

Paper 05207RR received Jul. 25, 2005; revised manuscript received Feb. 13, 2006; accepted for publication Feb. 13, 2006; published online May 12, 2006.

1 Introduction

Focal cerebral ischemia, clinically called stroke, may result in severe or lethal neurological deficits. Ischemia results from a transient or permanent reduction in cerebral blood flow that is restricted to the territory of a major brain artery.[1] Middle cerebral artery occlusion (MCAO) is usually used to model the focal cerebral ischemia in both rodents and primates.[2–6] Due to differences in residual cerebral blood flow (CBF) and metabolism, the ischemic hemisphere consists of an ischemic core (infarct), the ischemic penumbra, and normal tissue.[1,7] The ischemic penumbra is the transition zone between the normal tissue and the infarct, and may be either only reversibly damaged or destined to infarct. The primary goal of neuroprotection in focal cerebral ischemia is to salvage the penumbra.[1] The evolution of the ischemic penumbra into infarction is of particular interest.[7–9]

Many imaging techniques, including PET,[5,10] magnetic resonance imaging (MRI),[4,11] laser speckle contrast imaging,[12,13] near-infrared spectroscopy,[14,15] and autoradiography,[16,17] have been used to study focal cerebral ischemia. Previous studies have concentrated on the residual CBF and the water flow (movement of water in/out of cells) in the tissue. This work investigates how focal cerebral ischemia alters spontaneous spreading depression (SD) waves. SD is attracting intensive attention for its underlying role in ischemia.[18–24] Since SD waves that spread from the penumbral area have been shown to cause expansion of the infarct core,[16,19,21] electrophysiological recordings of SD waves have been used for acute and long-term monitoring of ischemia;[24] however, such recordings have inherently low spatial resolution. Optical intrinsic signal imaging (OISI), on the other hand, is a neuroimaging technique that can map a large region of cortex both with high temporal and spatial resolution.[25–29] OISI uses a charge-coupled device (CCD) camera to image optical reflectance at 550-nm wavelength, which is sensitive to SD wave propagation due to changes in regional cerebral blood volume (CBV). The deoxyhemoglobin and oxyhemoglobin have nearly the same absorbance at the 550-nm wavelength.[27] OISI has previously been applied to study SD in the normal cortex.[25–29] This work extends OISI to monitoring spontaneously developing SD in the ischemic cortex, and identifies patterns of optical change that characterize normal brain, the penumbra, and the infarct core. As a control, images of the SD waves in normal brain induced by a pinprick are also presented.

Address all correspondence to Qingming Luo, Huazhong University of Science and Technology, Dept. of Biomedical Engineering, The Key Lab of Biomedical Photonics-College of Life Science and Technology, Wuhan, Hubei 430074 China. Tel: 86 27 8779 2033; Fax: 86 27 8779 2034; E-mail: qluo@mail.hust.edu.cn

1083-3668/2006/11(3)/034002/13/$22.00 © 2006 SPIE

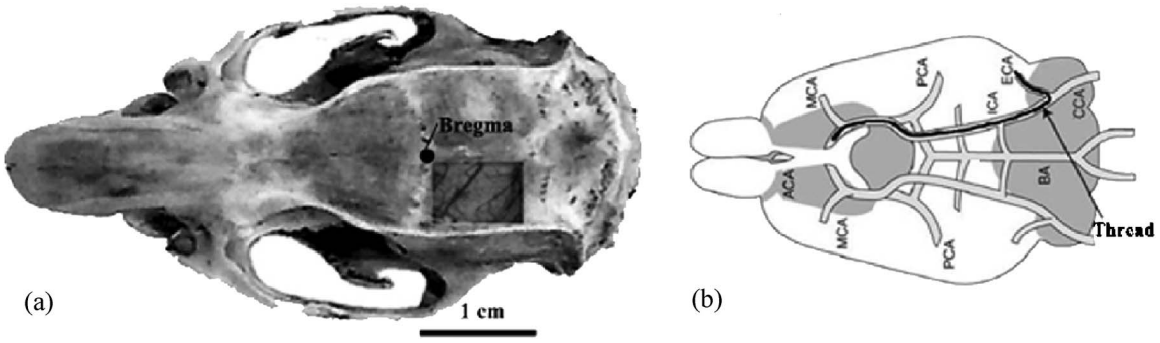

Fig. 1 (a) Top view of the rat skull. The rectangle shows the area of the thinned skull used for optical imaging, located just lateral to the Bregma. (b) A monofilament nylon thread was inserted into the ICA via the ECA to occlude the left medial carotid artery (MCA).

As a technical contribution, this work introduces a differential image method for processing the sequence of camera images to improve visualization of the SD waves. The customary OISI image in the neurological community is based on the following calculation:

$$A = \frac{I - I_o}{I_o}, \tag{1}$$

where I denotes the pixel values of the image at some time point, and I_o denotes the initial image just prior to the SD wave. The difference image is a rate-of-change image, and is calculated:

$$B = \frac{I(i) - I(i-1)}{I_o}, \tag{2}$$

where $I(i)$ refers to the image at the i'th time point, and $I(i-1)$ refers to the immediately previous image at the time point $i-1$. The B image is shown in this work to significantly enhance the leading and trailing edges of an SD wave, and to enhance the visualization of dilation and contraction of larger blood vessels. Both types of image, A and B, are in dimensionless units and easily compared among investigators. However, it is important to note the time step (Δt) between image frames when reporting B images. In this work, Δt was 6.4 s. Finally, a maximum rate-of-change image is calculated:

$$C = \max(B), \tag{3}$$

where the maximum value of each pixel in B over the ~3-min duration of a particular SD wave is determined and displayed. The C image is shown to visualize the entire penumbra region based on the vascular response during each SD wave. This work compares the A, B, and C images of normal, penumbra, and infarct areas in rat brains with MCAO-induced ischemia.

We also present an optical model for the brain tissue preparation that involves thinning the skull to a 100-μm thickness and covering it with silicone oil. The preparation allows direct viewing of the brain tissue without disturbance. However, the light scattered by the thin skull layer influences the interpretation of optical changes of reflectance in terms of volume changes in the microvasculature of the brain. The model allows proper interpretation.

2 Materials and Methods

2.1 *Animal Preparation*

Adult male Sprague-Dawley rats ($n=10$) weighing 250 to 350 g were anesthetized using an intraperitoneal injection of α-chloralose and urethane (50 and 600 mg/kg, respectively). The body temperature of the animal was monitored with a rectal temperature probe and maintained at 37.0 ± 0.5 °C using a heating regulator pad. The femoral artery and vein were cannulated for the recording of arterial blood pressure and infusion of saline solution, respectively. The arterial pO_2, pCO_2, and pH were measured periodically. The skull above the left parietal cortex was thinned to about 100 μm with a saline-cooled dental drill to form a "window" of 6×8 mm, centered at 4.3-mm caudal and 3.3-mm lateral to the bregma. The window was then filled with silicone oil to avoid heat loss and prevent the skull from drying. Permanent focal cerebral ischemia was then induced using Longa's method of intraluminal middle cerebral artery occlusion (MCAO).[3] For this procedure, the left carotid artery tree was isolated. A smooth monofilament nylon thread (diameter of 0.20 mm) was inserted from the lumen of the external carotid artery (ECA) into the internal carotid artery (ICA), with the advanced length being about 20 mm from the bifurcation of the common carotid artery (CCA) (see Fig. 1). All the monitored physiological parameters stayed within normal physiological range during the experiments. The mean arterial blood pressure (MABP) and blood gas values were as follows: MABP=98 ± 11 mmHg, $pO_2=145\pm14$ mmHg, $pCO_2=37\pm4$ mmHg, and pH=7.4 ± 0.1. Except for two rats, eight rats were found to present spontaneous SD waves within the 4-h period following MCAO. The statistical results shown here are based on the experiments performed in these eight rats, and the values are reported as mean±standard deviation, either for $n=8$ rats or for $n=16$ sites (8 rats$\times$2 sites/rat). As a control, one rat was prepared for imaging, but rather than an MCAO, the animal received a pinprick in the middle of the window to induce an SD wave. The one rat experiment repeats multiple previous pinprick experiments not shown here.

2.2 *Optical Imaging*

After skull preparation and MCAO, the rat was fixed in a stereotactic frame and transferred to the OISI imaging system, described previously,[30] which required 15 min. A light source

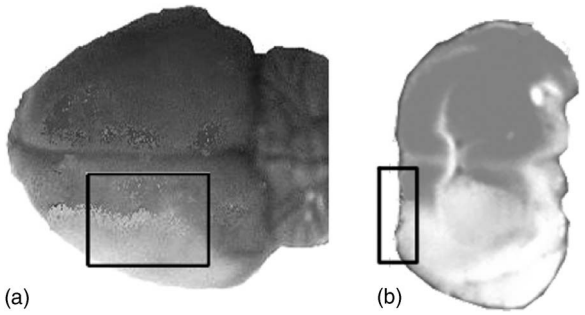

Fig. 2 Brain stained after MCAO procedure. (a) Top view of the rat brain. Rectangle shows region of optical imaging. (b) Transverse view shows normal brain in the medial region and infarct in the lateral region.

at 550±10 nm was used to illuminate the parieto-occipital cortex through the cranial window. Illumination was oblique (~30 deg off the normal to the brain surface) to avoid glare from the tissue surface. Image acquisition was performed using a 12-bit CCD camera (480×640 pixel resolution, Pixelfly, PCO Computer Optics, Germany) attached to a microscope (Olympus SZ6045TRCTV, Japan) observing an area of 6×8 mm. Images were captured every 6.4 s (each image was the average of 256 frames, each at a 25-ms exposure time) starting 15 min after MCAO. For each animal, 1000 images were collected continuously over a 2-h period and stored on a personal computer. After a delay of less than 5 min, another 1000 images were acquired. In total, ten rats following MCAO were imaged for about 4 h. Through visual inspection of the image sequences, eight rats were observed to develop SD waves, and two rats did not develop SD waves.

2.3 *Triphenyltetrazolium Chloride Staining*

Immediately after imaging, the ten animals were sacrificed and their brains removed from the cranium. Five brains, two of which did not present SD waves, were immersed in a 2% solution of 2,3,5-triphenyltetrazolium chloride (TTC) at 37°C. After 30 min, the dorsal sides of these brains were imaged. The other five brains were cut into coronal slices at 3-mm intervals, immersed in a 2% solution of TTC, and incubated for 30 min at 37 °C. Images of the stained sections were then recorded. Figure 2 shows the MCAO-induced ischemic region stained by TTC.

2.4 *Calibration of In Vivo Rat Brain Reflectance*

The images of rat brain based on the intensity of reflected light were acquired in laboratory units of (counts/pixel), referred to as I. After inducing the stroke and transferring the animal to the microscope, an image just prior to the first SD wave was acquired and called I_o. An image of a white plastic reflectance standard, calibrated to be $R_{\text{std}}=0.95$ at 550 nm in separate experiments, was acquired, and is referred to as I_{std}. The dark current of the camera was determined (72 counts/pixel) and is referred to as D_k. The reflectance (R) of the rat brain was calculated, $R=R_{\text{std}}(I_o-D_k)/(I_{\text{std}}-D_k)$, yielding a reflectance image in dimensionless units [Fig. 3(a)]. The values of reflectance for five pixels (circles) on a central 195-μm-diam artery ($R=0.066\pm0.002$, mean±standard deviation) and five pixels (squares) on brain tissue with only microvasculature (no large blood vessel) ($R=0.134\pm0.012$) were obtained.

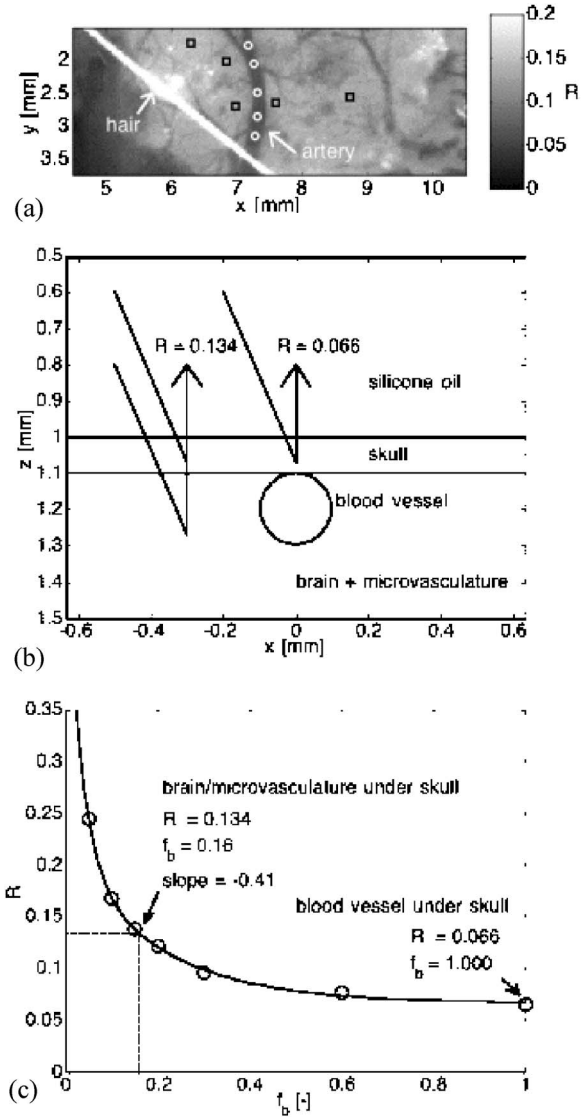

Fig. 3 Optical model of the thinned skull preparation for brain imaging experiments. (a) Calibrated reflectance image of local region of interest within field of view, showing a 195-μm-diam artery. A hair enabled focusing during imaging of the reflectance standard, and artifactually appears white in this reflectance image. Circles and squares denote the sites along the artery and the sites in the brain without any large artery or vein but only microvasculature, respectively, where reflectance values were recorded. The mean (± standard deviation) reflectance of the artery and brain/microvasculature was 0.066±0.001 and 0.134±0.012, respectively, at 500-nm wavelength. (b) The geometry of the model for the thinned skull preparation. (c) The reflectance (R) of the brain/microvasculature sites as a function of the blood volume fraction (f_b) of the microvasculature based on Monte Carlo simulations. When $f_b=0.16$, the predicted R matches the observed R of 0.134. The significance of this model is that a 10% increase in reflectance in OISI images corresponds to a 21% decrease in microvasculature blood volume.

2.5 *Optical Model for Brain Preparation*

An optical model for the rat brain preparation was specified by the previously mentioned reflectance values (Fig. 3(b)).

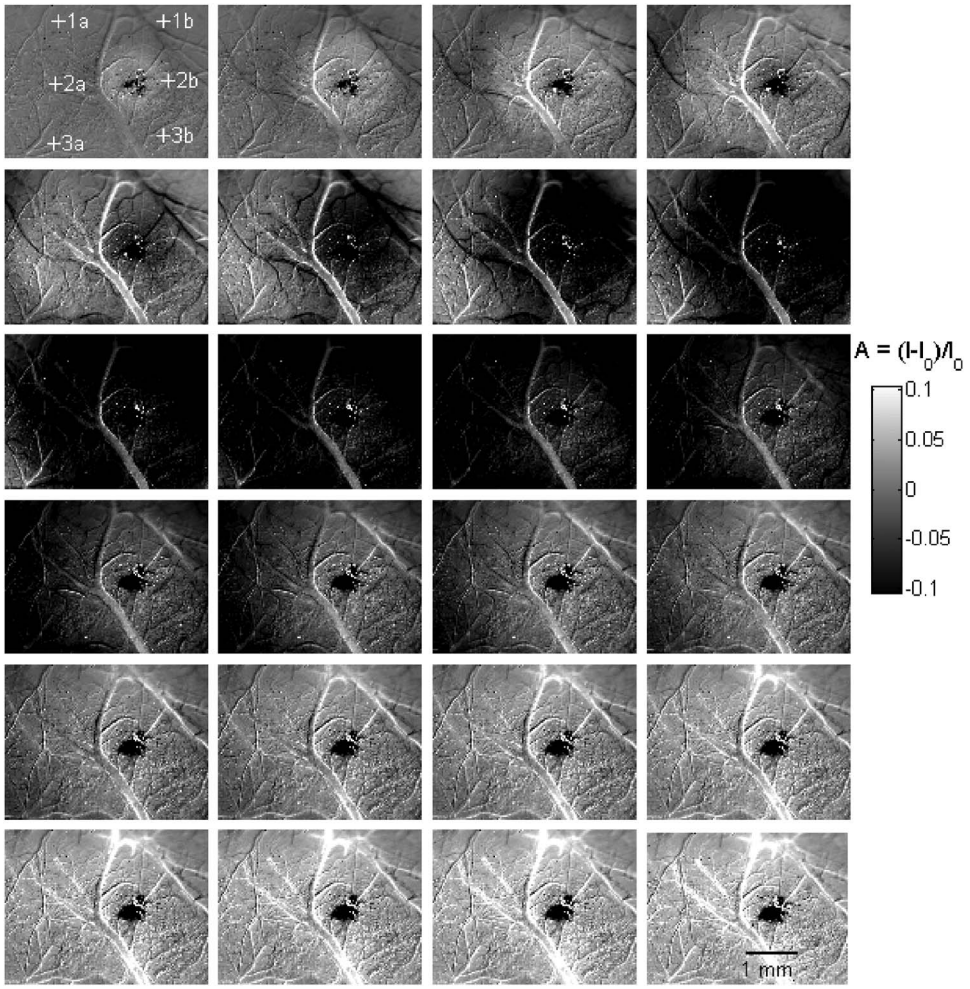

Fig. 4 Image series of a pinprick-induced spreading depression (SD) wave in normal brain [*A* images of relative reflectance, see Eq. (1)]. The region of the pinprick remains dark due to direct vascular trauma. An SD wave originates at the pinprick and spreads radially, presenting a bright region of increased reflectance due a decrease in cerebral blood volume (CBV). A subsequent region of hyperperfusion occurs at the pinprick and spreads radially, presenting a dark region of decreased reflectance due to increased CBV. Each image is separated by 6.4 s. Scale is ±0.10, or ±10% changes in reflectance.

Table 1 Parameters of optical model for the thinned-skull brain preparation. The refractive index (n), blood volume fraction (f_b), oxygen saturation of hemoglobin (S), absorption coefficient (μ_a), scattering coefficient (μ_s), anisotropy of scattering (g), and thickness or diameter (d), of tissue layers or structures are in the Monte Carlo model of the tissue preparation. The model mimics the behavior of Fig. 3(a) and the model geometry is shown in Fig. 3(b).

Tissue	n	f_b	S	μ_a [cm^{-1}]	μ_s [cm^{-1}]	g	d [cm]
Silicone oil	1.5	0	0	0	0	0	0.1
Skull (bloodless)	1.37	0	0	0.001	580	0.90	0.0100
Blood vessel	1.37	1	0.95	259	240	0.95	0.0200 diam
Brain/microvasculature	1.37	0.16	0.93	63	401	0.84	1.0

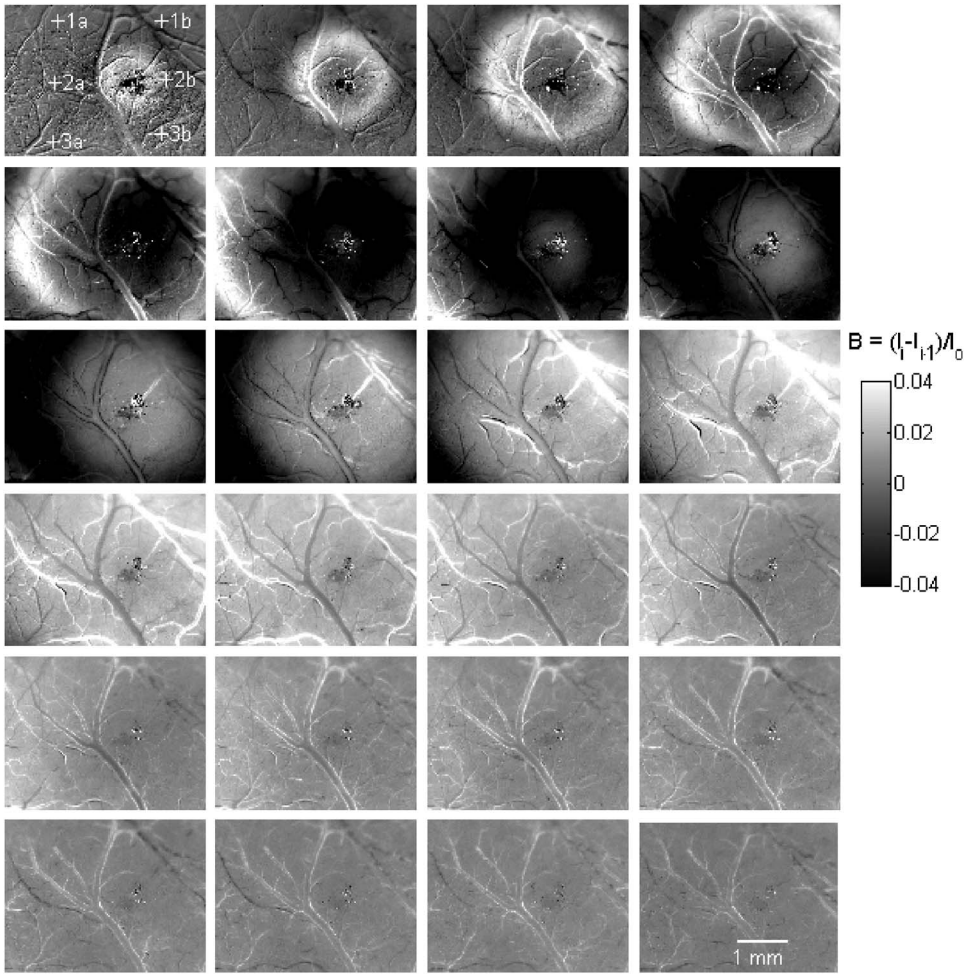

Fig. 5 Image series of a pinprick-induced spreading depression (SD) wave in normal brain [B images of rate of change in reflectance, see Eq. (2)], same progression as Fig. 4. The *B* images are rate-of-change images that highlight the leading and trailing edges of the SD wave. Scale is 4% change in reflectance per 6.4-s time interval.

The brain preparation was modeled as a homogeneous brain tissue with microvasculature, a large (195 μm diam) superficial blood vessel, a 100-μm-thick skull, a 1-mm-thick layer of clear silicone oil, and a silicone-air surface boundary. A Monte Carlo computation was adapted to simulate this model.[34] The optical properties of the components of the model were specified (μ_a=absorption coefficient [cm^{-1}], μ_s =scattering coefficient [cm^{-1}], g=anisotropy). The optical properties of whole blood at 550 nm were assigned to the 195-μm-diam blood vessel in Fig. 3(a) (μ_a=259 cm^{-1}, μ_s =240 cm^{-1}, and g=0.95, for oxygen saturation of S=0.93).[35] The value of μ_s for the skull was adjusted, holding the values g=0.90 and μ_a=0.001 cm^{-1} constant, until the reflectance from the skull above the vessel reached the measured 0.066 value. The result for the skull was μ_s=448 cm^{-1}, with g set equal to 0.90 and μ_a=0.001. Then, the optical properties were determined for the underlying brain tissue away from the blood vessel but with an overlying skull layer, by varying the blood volume fraction (f_b) of the brain tissue while holding the scattering properties of the brain constant, until the reflectance matched the measured 0.134 value. The oxygen saturation of the mixed arterio-venous microvasculature was held constant at S=0.90. The optical scattering properties for brain plus microvasculature were assigned values based on the linear combination of a fraction f_b of whole blood and a fraction of $(1-f_b)$ of bloodless brain tissue. Properties for bloodless brain were estimated (μ_a=0.001, μ_s=410 cm^{-1}, g=0.82) from literature reports.[36,37] The result for the brain tissue that matched the 0.134 reflectance was f_b=0.16, S =0.90, μ_a=40.3 cm^{-1}, μ_s=401 cm^{-1}, and g=0.84. Figure 3(b) shows the model geometry, and Table 1 summarizes the model parameters. While a more careful study should fully explore the optical properties of this tissue preparation, the prior preliminary model is sufficiently accurate to allow an interpretation of changes in reflectance in acquired OISI images in terms of changes in microvasculature blood volume fraction (f_b). Figure 3(c) shows the relationship between the reflectance of the brain plus microvasculature with the thinned overlying skull versus the blood volume fraction of the microvasculature. The slope $\Delta R/\Delta f_b$ at the experimentally observed data point (f_b=0.16, R=0.134) is −0.41. Therefore, when a 10% increase in reflectance (ΔR=0.10R=0.0134) is seen in an A image, the corresponding change in the volume

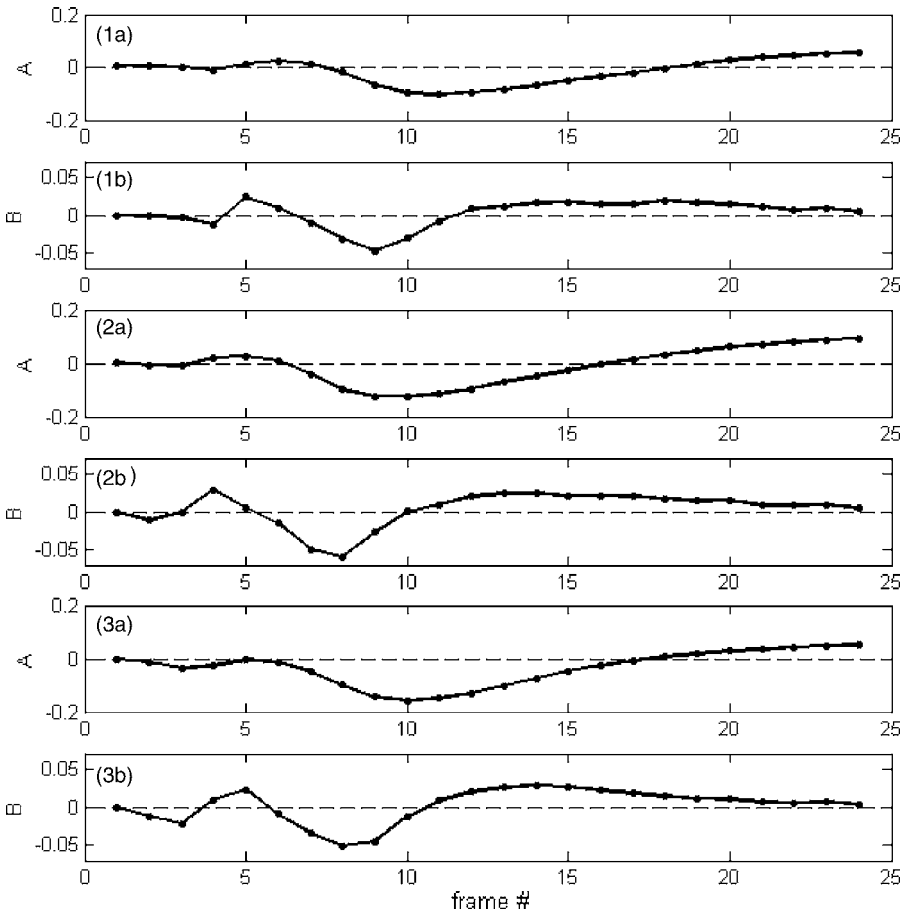

Fig. 6 Time course of *A* and *B* signals from pinpricked-induced SD wave from three sites corresponding to medial, intermediate, and lateral positions in the field of view (labeled 1a, 2a, and 3a corresponding to sites in Figs. 3 and 4). The signals from the three sites are very similar, as expected for normal brain.

fraction of microvasculature should have decreased 21% ($\Delta f_b = 0.21 f_b = 0.033 = 0.0134/0.41$).

2.6 *Image Processing*

The sequences of images of the normal and ischemic rat brains were processed as described in the Introduction in Sec. 1 to yield *A* images, $A=(I-I_o)/I_o$; *B* images, $B=[I(i)-I(i-1)]/I_o$; and *C* images, $C=\max(B)$. The *A* images are the form usually reported in the neuroscience literature. The *B* images are introduced to offer better contrast when visualizing the leading and trailing edges of an SD wave. The *C* images are introduced to better visualize the entire penumbra. 24 image frames distributed evenly throughout the ~3-min period of a single SD wave in both normal brain and in ischemic brain were chosen for display. Also, six positions in each frame were chosen for display of the time dynamics of the tissue reflectance, two in each of the three areas, 1 =normal brain in the medial dorsal region, 2=penumbra in the intermediate cortex that transitions between normal and infarct, and 3=infarct in the lateral region where the ischemic core is located. Two points for each area were chosen for display to illustrate the degree of reproducibility in the signals. The time points extended over 3 min for the normal brain to display one SD wave induced by a pinprick, and over a 4-h period for the ischemic brain to display the cyclic pattern of multiple spontaneous SD waves. The signals in a 5 ×5 pixel region of interest centered on each of the six chosen positions were averaged for this display. To demonstrate the maximum rate-of-change image of the penumbra, *C* images were prepared for the first three SD waves in one rat.

3 Results

3.1 *Spreading Depression Waves in Normal Rat Brain Induced by Pinprick*

Figures 4–6 show the time course over a 3-min period of a single SD wave induced by a pinprick in a normal rat brain. Figure 4 shows the customary image, $A=(I-I_o)/I_o$. Figure 5 shows the differential image, $B=[I(i)-I(i-1)]/I_o$. Figure 6 shows a plot of the time course of reflectivity expressed as both *A* and *B* signals, presenting one example from each of the three regions (traces show regions labeled as 1a, 2a, and 3a in Figs. 4 and 5) that in later experiments will be associated with the normal, penumbra, and infarct areas of the MCAO-induced ischemic brain. The traces illustrate that the *A* and *B* images of the three regions in normal brain behave the same in response to pinprick-induced SD waves.

In Fig. 4, the *A* images (change in reflectance) show an initial increase in reflectivity as the SD wave propagates due to vasculature contraction, followed by darkening as hyper-

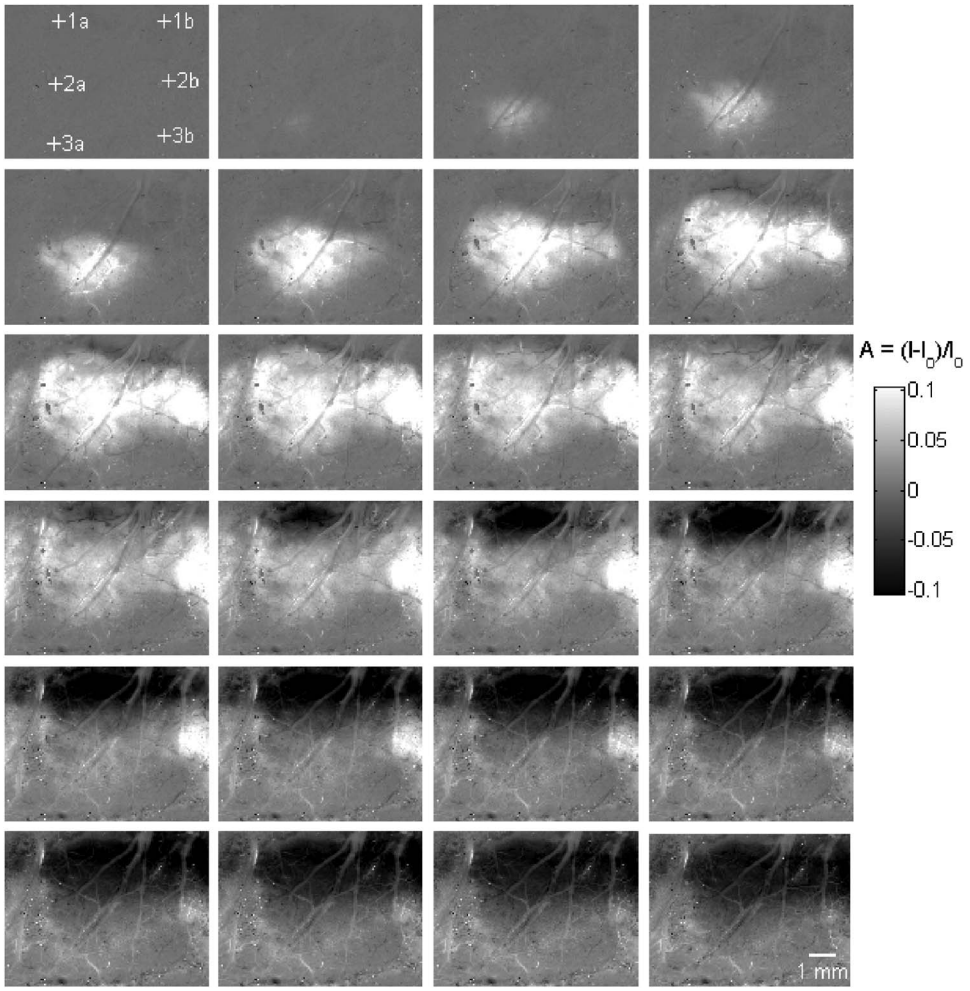

Fig. 7 Image sequence of an ischemia-induced SD wave in brain after MCAO procedure (*A* images of relative reflectance), showing one SD wave. Top region is normal brain (contains sites 1a and 1b), intermediate region is penumra (2a and 2b), and the lower region is the infarct area (3a and 3b). The SD wave originates in the penumbra, presenting a white region of increased reflectance due to a drop in cerebral blood volume (CBV). Subsequently, normal brain darkens quickly as reflectance drops below the initial reflectance level due to the hyperperfusion. In contrast, the penumbra returns slowly to normal reflectance with very little hyperperfusion. The infarct area shows no changes.

perfusion occurs, then a slow return to normal values. This behavior is consistent with behavior cited in previous reports.[27,29] The pinprick itself remains dark, presumably due to local inflammatory vasodilation due to tissue damage. A large artery traverses the field of view and appears white because it is contracting, decreasing its blood volume and allowing more reflected light from underlying tissue to escape to the camera. The edges of the blood vessel look especially white in early frames (e.g., 3, 4, and 5), consistent with contraction of the vessel. In later frames, the vessels again dilate and return to a gray color.

In Fig. 5, the *B* images (rate of change in reflectance) show the same information but with several advantages. 1. The leading edge and trailing edge of the SD wave are significantly sharpened, allowing the SD wave to be more clearly visualized. 2. Sudden contraction of the artery presents as a vessel with a bright outer edge (e.g., frames 3, 4, and 5), as the reflectance at the vessel edge increases due to the drop in blood volume in those pixels. 3. Sudden dilation of larger blood vessels presents as a vessel with a dark outer edge, as the reflectance drops at the vessel edge (e.g., frames 4, 5, and 6). 4. The *A* images tend to appear saturated, either as light areas of decreased blood volume or dark areas of increased blood perfusion, while *B* images better avoid saturation and remain responsive to changes in blood volume.

Figure 6 shows the time course of a single SD wave induced by a pinprick in normal rat brain for the three positions (1a, 2a, and 3a) shown in the first frame of Figs. 4 and 5. Both the *A* and *B* signals are plotted. The time dynamics at a particular point were able to discriminate a brief initial drop of reflectance ($-3.6\pm1.0\%$, $n=16$ sites), indicating a brief hyperperfusion. Then, the standard pattern seen in Figs. 4 and 5 occured. There was a rise in reflectance ($1.1\pm1.6\%$) as perfusion decreased, then a strong drop in reflectance ($-15\pm3.9\%$) as a hyperperfusion developed (see Table 2). Finally, there was a recovery toward zero as normal perfusion was restored. The associated *B* measurements present the time derivative of the *A* values, in other words positive when *A* was increasing and negative when *A* was decreasing. All the

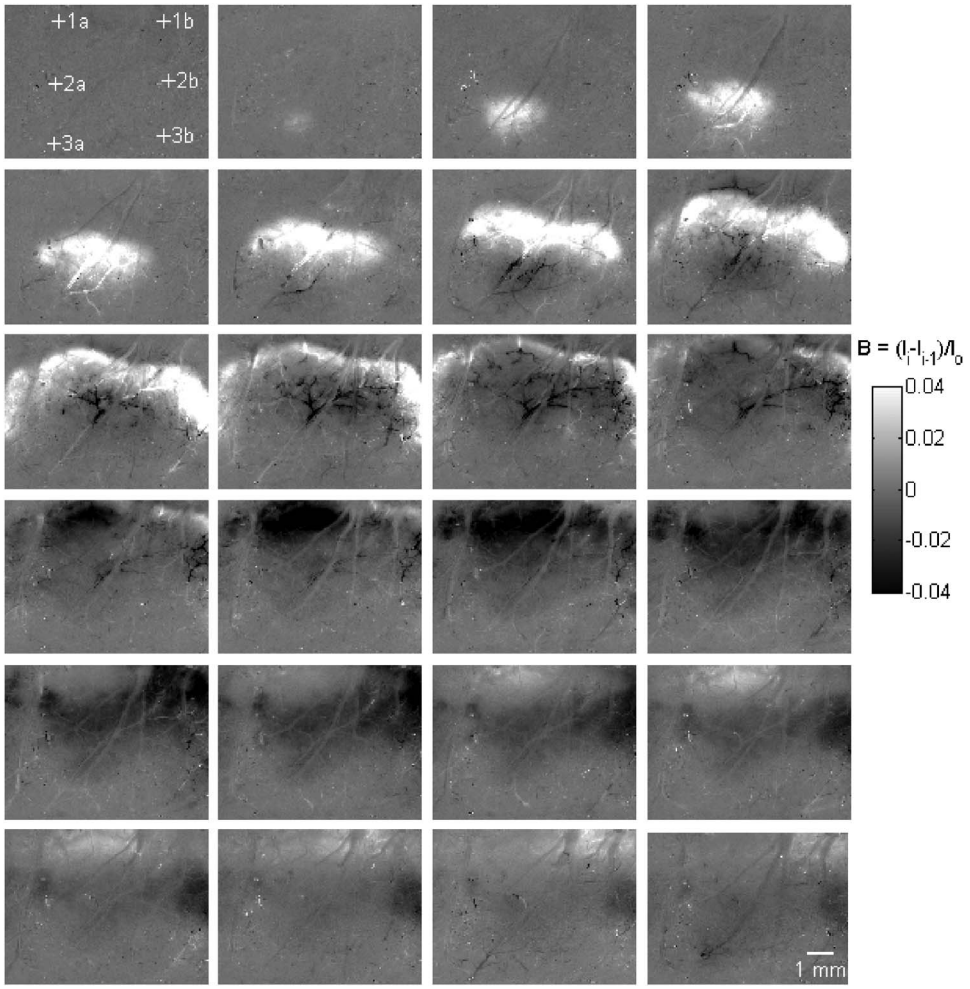

Fig. 8 Image sequence of an ischemia-induced SD wave in brain after MCAO procedure (*B* images of rate of change of reflectance). The *B* images highlights the changes seen in Fig. 7.

traces for positions 1a, 2a, and 3a were similar because this was a normal brain.

3.2 *Spontaneous Spreading Depression Waves in Ischemic Rat Brain*

Following MCAO to induce a region of ischemia in each animal, a series of n spontaneous SD waves ($n=10\pm4$), each roughly 3 min in duration, developed during the 4-h period of image acquisition. Figures 7–9 show the time course of one SD wave (the second SD wave in a series of 15 SD episodes experienced by this rat).

In Fig. 7, the *A* images showed that the behavior in regions 1 (normal), 2 (penumbra), and 3 (infarct) differed. In region 1 (normal), the *A* images show an initial increase in reflectivity (decrease in blood) in the medial cortical region near the midline (0.3 to 2-mm lateral), followed by a dark region of hyperperfusion. This behavior was similar to that seen in the pinprick-induced SD of normal brain. In region 2 (penumbra), the initial increase in reflectivity is seen, but the hyperperfusion does not significantly occur and the reflectivity only slowly recovers to the baseline value. In region 3 (infarct), there is little change in the reflectivity over the measurement time period.

Figure 8 shows the *B* images of the MCAO-induced SD waves. In region 1 (normal), the *B* images clearly show the movement of an SD wave, with an initial rising reflectivity (white area) followed by a decreasing reflectivity (dark area). In the leading edge of the SD wave, the perfusion was dropping rapidly, which caused the leading edge to appear white in these difference images. In the trailing edge of the SD wave, the perfusion was increasing rapidly, a hyperperfusion that caused the trailing edge to appear dark in these difference images (e.g., frames 7 through 12). After this hyperperfusion, the blood perfusion recovered, which caused the region to appear white during this recovery period. In region 2 (penumbra), there was an initial rapidly rising reflectivity that appeared white, but only a slow recovery toward normal perfusion without any hypeperfusion, and this recovery was too slow to cause the difference image to be very white, so it remained relatively gray. In region 3 (infarct), there were no changes in reflectivity. The SD wave did not invade the infarcted area.

Figure 9 shows the time course of a single SD wave in the ischemic rat brain for the three positions (1a, 2a, and 3a) shown in the first frame of Figs. 7 and 8. In region 1 (normal), the behavior is like the normal rat brain (Fig. 6). There was an

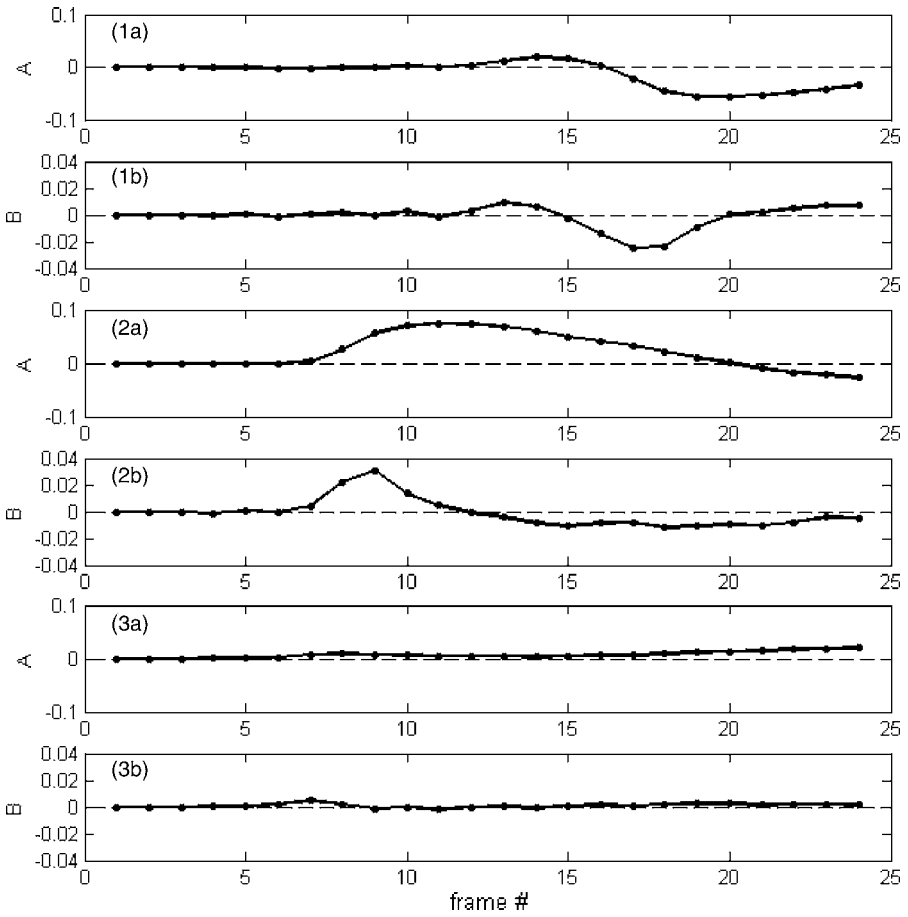

Fig. 9 Time course of *A* and *B* signals from an ischemia-induced SD wave corresponding to normal brain, penumbra, and infarct (labeled 1a, 2a, and 3a corresponding to sites in Figs. 3 and 4). The penumbra shows a rapid initial rise in the rate-of-change *B* signal (frames 7, 8, and 9) that is a signature for the penumbra, corresponding to a rapid constriction of blood volume. The normal brain does not present this initial rise in *B* signal, but later shows a drop in *B* signal (frames 16 through 19) due to hyperperfusion. The infarct does not change.

initial rise in reflectivity ($3.0\pm2.6\%$, $n=16$ sites on eight rats) due to a drop in blood perfusion, followed by a decrease in reflectivity ($-12.5\pm2.8\%$) due to hyperperfusion. Then, the vessels recovered and normal reflectance was restored. In region 2 (penumbra), the initial increase in reflectance was stronger ($12.1\pm3.6\%$) as blood perfusion dropped. However, the penumbra did not experience the strong hyperperfusion seen in normal brain, but showed only a slight drop in reflectivity ($-4.1\pm2.1\%$) (see Table 2). Then, reflectance recovered toward normal levels. In region 3 (infarct), there were no changes in reflectivity due to SD waves, although the reflectance slowly increased ($3.1\pm2.5\%$). The *B* images highlighted this behavior. The initial penumbra response was especially strong, showing a rapid decrease in perfusion recorded as a strong rising reflectance.

Figure 10 shows the full time course of *A* signals over the 400-s period of imaging in the normal brain with a pinprick-induced SD wave. The horizontal bar shows the portion of the time course that appeared in Fig. 6. Figure 10 shows the *A* signals of all six positions, 1a, 1b, 2a, 2b, 3a, and 3b (specified in the first frame of Figs. 4 and 5). The purpose of this figure is to illustrate the degree of reproducibility in such signals.

Figure 11 shows the full time course of *A* signals over the 4-h period of imaging in the ischemic brain. The short horizontal bar at ~0.5 h shows the portion of the time course that appeared in Fig. 9. Figure 11 shows all six positions, 1a, 1b, 2a, 2b, 3a, and 3b (specified in the first frame of Figs. 8 and 9). There was a 5-min break in data acquisition at 2 h. In positions 1a and 1b (normal), the first 2 h of SD waves showed an initial rise in reflectance, followed by a pronounced drop in reflectance. In the latter 2 h, the initial rise in reflectance did not occur, but the strong drop in reflectance continued to be a reliable indicator of SD waves. In positions 2a and 2b (penumbra) in the first 2 h, the initial rise in reflectance during each SD wave was stronger than in normal brain, but in the latter 2 h the rise was greatly diminished. There was no drop in reflectance in the penumbra. In positions 3a and 3b (infarct), only a very slight transient rise in reflectance was apparent with some SD waves, but in general the infarct was nonresponsive to SD waves.

Figure 12 presents the *C* images (maximum rate-of-change in reflectance) that visualized the entire penumbra. As a single SD wave propagated across the brain, the sequence of images recorded the time-resolved history of that propagation. View-

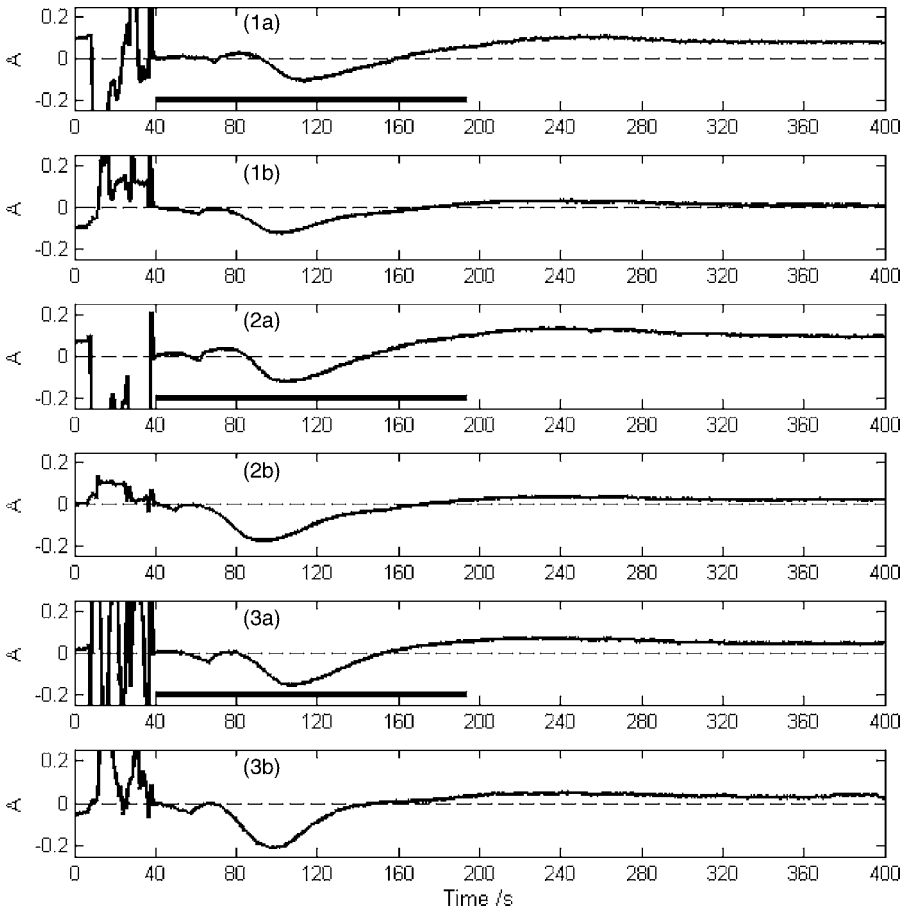

Fig. 10 Time course of pinprick-induced *A* signals for six sites (1a, 1b, 2a, 2b, 3a, and 3b, in Figs. 3 and 4) to illustrate the reproducibility of the SD wave signals. Horizontal bar shows the time domain of data shown in Fig. 6.

ing the sequence as the rate-of-change *B* images, the *B* value of each pixel as a function of time was accessed and the maximum *B* value of that pixel assigned to the *C* image. Hence, the *C* image was a maximum rate-of-change image. Figure 12(a) shows an initial image in the laboratory units of counts/pixel. Figures 12(b) and 12(c) show the *C* images of the first, second, and third SD waves. Both the normal brain and the infarct area appeared dark, while the penumbra appeared bright. One can observe the penumbra-infarct boundary progressing slowly into the penumbra, as the infarct grows and the penumbra shrinks, while the penumbra-normal boundary remains constant.

4 Discussion

The aim of this work is to present new methods of preparing OISI images that enhanced the contrast of SD waves. This work presents three types of images derived from the same sequence of intensity images: *A* images that indicated the change in reflectance, *B* images that indicated regions of rapid change in reflectance and enhanced the leading and trailing edges of the SD wave, and *C* images that indicated the maximum rate of chage in reflectance per 6.4-s time interval over the time duration of a single SD wave and visualized the penumbra.

This work also presents an optical model of the thinned skull model employed for the OISI imaging. Such an optical model enables proper interpretation of changes in reflectance in terms of the true changes in microvascular blood volume fraction. The optical images of reflected intensity were calibrated to yield reflectance images. The values of reflectance from an area with a large blood vessel versus an area lateral to the blood vessel allowed specification of the model (see Fig. 3 and Table 1), which described the brain preparation as a homogeneous brain tissue with microvasculature, a typical superficial large blood vessel (195 μm-diam), an overlying 100-μm-thick skull, an outer 1-mm layer of silicone oil, and a silicone/air surface. The model allows the observed changes in *A* images to be interpreted in terms of changes in blood volume fraction (f_b) of the brain microvasculature. The resting brain had a reflectance of 0.134 with a microvasculature blood volume fraction (f_b) of 0.16. A 10% increase in *R* corresponded to a 21% decrease in f_b. The optical model presented in this work is preliminary, and more work should be done. The blood volume fraction of 0.16 seems quite high, although optical measurements are relatively superficial and the blood content of the outer layer of the cortex may have a higher local perfusion than the average brain perfusion. The literature values for scattering properties of brain at 550 nm were based on autopsy samples of human brain. We have

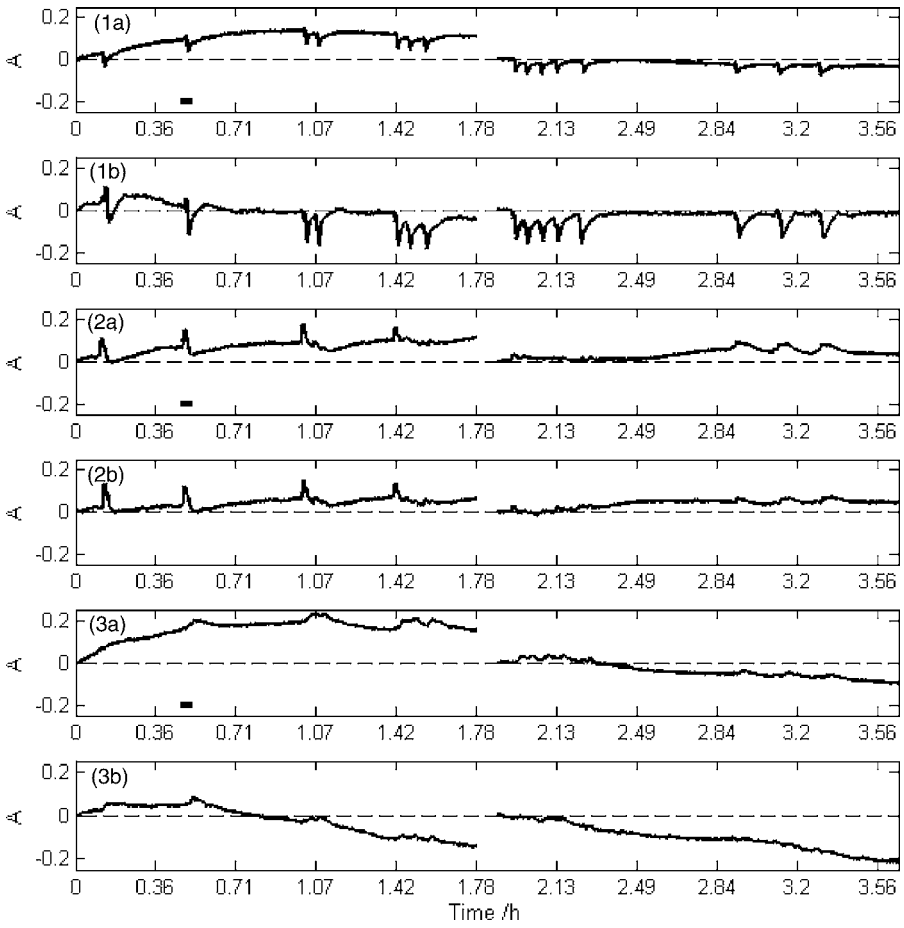

Fig. 11 Time course of ischemia-induced *A* signals for six sites (1a, 1b, 2a, 2b, 3a, and 3b in Figs. 3 and 4) to illustrate the reproducibility of the SD wave signals. Horizontal bar shows the time domain of data shown in Fig. 9.

observed that optical scattering of brain in mice drops rapidly upon excision. So, more work is needed. Nevertheless, the model provides an initial estimate of the quantitative change in perfusion associated with a measured change in reflectance in OISI.

4.1 *Relevance of Optical Signals to Ischemia*

For wavelengths around 550 nm, the reflectance signal of SD waves primarily reflected the local cerebral blood volume (CBV) change. Roughly, a decrease of reflectance signal indicated an increase of local CBV, and an increase of signal represented a decrease of CBV. Previous work has suggested that the dramatic hyperperfusion during the induced SD in normal cortex is a cause for the increase in CBV.[26,27] This work illustrates the time progression of an initial increase in reflectance due to contraction of vasculature, followed by a more pronounced drop in reflectance due to the previously reported hyperperfusion as blood vessels overdilate. However, this classic response was not uniform in the MCAO-induced ischemic brain. This work indicates that the penumbra showed an enhanced initial increase in reflectance due to microvasculature contraction, but the vessels did not subsequently overdilate and only slowly recovered toward normal. The infarct area showed no significant changes in reflectance. The hemodynamic responses during spontaneous SD waves depend on the residual cerebral blood flow (CBF).[31,32] In the area of normal perfusion, the metabolic workload of SD wave propagation is coupled to a simultaneous increase in CBF, so the CBV also shows an increase. In the penumbral area, the decrease of CBV is related to reduced microcirculation associated with spontaneous SD.[33]

Table 2 Summary of changes in reflectance in different regions of brain.

Tissue	Initial increase in *R*	Later decrease in *R*
Pinpricked normal brain	1.1±1.6%	−15±3.9%
SD, normal brain	3.0±2.6%	−12.5±2.8%
SD, penumbra	12.1±3.6%	−4.1±2.1%
SD, infarct	none	none

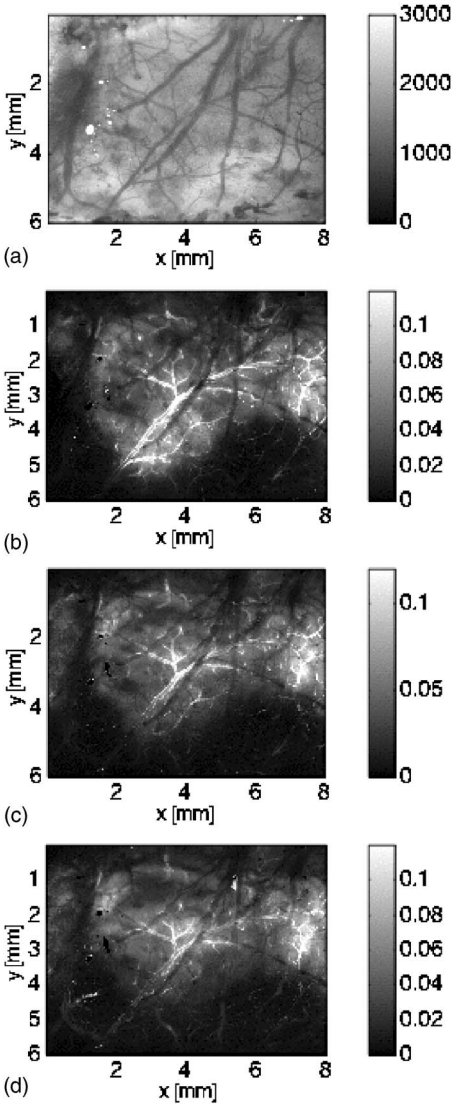

Fig. 12 Maximum rate-of-change images [*C* images, see Eq. (3)] of the first three SD waves induced by ischemia. (a) Original image just prior to first SD wave, shown in units of counts/pixel. (b) First SD wave, as *C* image. (c) Second SD wave. (d) Third SD wave. Each wave requires about 3 min to propagate over the field of view. These *C* images show the maximum *B* signal of each pixel over that time duration. The penumbra (intermediate region of image) shows bright, because each SD wave elicits a rapid initial rise in reflectance due to a sudden constriction of microvasculature. The normal brain (top rgion) and infarct (lower region) remain dark. Note that the lower penumbra-infarct boundary is slowly moving upward in (b), (c), and (d), indicating the slow expansion of the infarct and shrinkage of the penumbra. The upper penumbra-normal boundary is stable.

Acknowledgments

This work was supported by the National Natural Science Foundation of China (grant number 60478016), Major Program of Science and Technology Research of Ministry of Education (grant number 10420), Joint Research Fund for Overseas Chinese Young Scholars (grant number 30328014), and the National Institutes of Health (R01-EB000224). The help of Ralf B. Schulz in revising the manuscript is gratefully acknowledged.

References

1. U. Dirnagl, C. Iadecola, and M. A. Moskowitz, "Pathobiology of ischaemic stroke: an integrated view," *Trends Neurosci.* **22**(9), 391–397 (1999).
2. G. Z. Feuerstein and X. Wang, "Animal models of stroke," *Mol. Med. Today* **6**, 133–135 (2000).
3. E. Zea-Longa, P. Weinstein, S. Carlson, and R. Cummins, "Reversible middle cerebral artery occlusion without craniectomy in rats," *Stroke* **14**, 164–187 (1989).
4. K. Takano, L. L. Latour, J. E. Formato, R. A. Carano, K. G. Helmer, Y. Hasegawa, C. H. Sotak, and M. Fisher, "The role of spreading depression in focal ischemia evaluated by diffusion mapping," *Ann. Neurol.* **39**(3), 308–318 (1996).
5. P. Frykholm, J. L. R. Andersson, J. Valtysson, H. C. son Silander, L. Hillered, and L. Persson, "A metabolic threshold of irreversible ischemia demonstrated by PET in a middle cerebral artery occlusion-reperfusion primate model," *Acta Neurol. Scand.* **102**(1), 18–26 (2000).
6. A. J. Strong, S. E. Smith, D. J. Whittington, B. S. Meldrum, A. A. Parsons, J. Krupinski, A. J. Hunter, and S. Patel, "Factors influencing the frequency of fluorescence transients as markers of peri-infarct depolarizations in focal cerebral ischemia," *Stroke* **31**, 214–222 (2000).
7. K. A. Hossmann, "Viability thresholds and the penumbra of focal ischemia," *Ann. Neurol.* **36**(4), 557–565 (1994).
8. O. W. Witte, H. J. Bidmon, K. Schiene, C. Redecker, and G. Hagemann, "Functional differentiation of multiple perilesional zones after focal cerebral ischemia," *J. Cereb. Blood Flow Metab.* **20**, 1149–1165 (2000).
9. W. D. Heiss, "Experimental evidence of ischemic thresholds and functional recovery," *Stroke* **23**, 1668–1672 (1992).
10. S. Pappata, M. Fiorelli, T. Rommel, A. Hartmann, C. Dettmers, T. Yamaguchi, H. Chabriat, J. B. Poline, C. Crouzel, L. D. Giamberardino, and J. C. Baron, "PET study of changes in local brain hemodynamics and oxygen metabolism after unilateral middle cerebral artery occlusion in baboons," *J. Cereb. Blood Flow Metab.* **13**(3), 416–424 (1993).
11. Q. Shen, X. Meng, M. Fisher, C. H. Sotak, and T. Q. Duong, "Pixel-by-pixel spatiotemporal progression of focal ischemia derived using quantitative perfusion and diffusion imaging," *J. Cereb. Blood Flow Metab.* **23**(12), 1479–1488 (2003).
12. A. K. Dunn, H. Bolay, M. A. Moskowitz, and D. A. Boas, "Dynamic imaging of cerebral blood flow using laser speckle," *J. Cereb. Blood Flow Metab.* **21**, 195–201 (2001).
13. C. Ayata, A. K. Dunn, and Y. Gursoy-Özdemir, "Laser speckle flowmetry for the study of cerebrovascular physiology in normal and ischemic mouse cortex," *J. Cereb. Blood Flow Metab.* **24**, 744–755 (2004).
14. T. Wolf, U. Lindauer, U. Reuter, T. Back, A. Villringer, K. Einhaupl, and U. Dirnagl, "Noninvasive near infrared spectroscopy monitoring of regional cerebral blood oxygenation changes during peri-infarct depolarizations in focal cerebral ischemia in the rat," *J. Cereb. Blood Flow Metab.* **17**(9), 950–954 (1997).
15. J. P. Culver, T. Durduran, D. Furuya, C. Cheung, J. H. Greenberg, and A. G. Yodh, "Diffuse optical tomography of cerebral blood flow, oxygenation, and metabolism in rat during focal ischemia," *J. Cereb. Blood Flow Metab.* **23**, 911–924 (2003).
16. M. Nedergaard and J. Astrup, "Infarct rim: effect of hyperglycemia on direct current potential and [14C]2-deoxyglucose phosphorylation," *J. Cereb. Blood Flow Metab.* **6**(5), 607–615 (1986).
17. M. Ginsberg, L. Belayev, W. Zhao, P. W. Huh, and R. Busto, "The acute ischemic penumbra: topography, life span, and therapeutic response," *Acta Neurochir.* **73**(suppl), 45–50 (1999).
18. G. G. Somjen, "Mechanisms of spreading depression and hypoxic spreading depression-like depolarization," *Physiol. Rev.* **8**, 1065–1096 (2001).
19. K. A. Hossmann, "Periinfarct depolarizations," *Cerebrovasc Brain Metab. Rev.* **8**(3), 195–208 (1996).
20. H. Nallet, E. T. MacKenzie, and S. Roussel, "The nature of penumbral depolarizations following focal cerebral ischaemia in the rat," *Brain Res.* **842**, 148–158 (1999).
21. G. Mies, T. Iijima, and K. A. Hossmann, "Correlation between peri-infarct DC shifts and ischaemic neuronal damage in rat," *NeuroReport* **4**(6), 709–711 (1993).
22. R. Gill, P. Andine, L. Hillered, L. Persson, and H. Hagberg, "The

effect of MK-801 on cortical spreading depression in the penumbral zone following focal ischaemia in the rat," *J. Cereb. Blood Flow Metab.* **12**(3), 371–379 (1992).
23. T. Otori, J. H. Greenberg, and F. A. Welsh, "Cortical spreading depression causes a long-lasting decrease in cerebral blood flow and induces tolerance to permanent focal ischemia in rat brain," *J. Cereb. Blood Flow Metab.* **23**(1), 43–50 (2003).
24. V. I. Koroleva and J. Bures, "The use of spreading depression waves for acute and long-term monitoring of the penumbra zone of focal ischemic damage in rats," *Proc. Natl. Acad. Sci. U.S.A.* **93**, 3710–3714 (1996).
25. R. S. Yoon, P. W. Tsang, F. A. Lenz, and H. Kwan, "Characterization of cortical spreading depression by imaging of intrinsic optical signals," *NeuroReport* **7**, 2671–2674 (1996).
26. A. M. O'Farrell, D. E. Rex, A. Muthialu, N. Pouratian, G. Wong, A. Cannestra, J. Chen, and A. Toga, "Characterization of optical intrinsic signals and blood volume during cortical spreading depression," *NeuroReport* **11**, 2121–2125 (2000).
27. A. M. Ba, M. Guiou, N. Pouratian, A Muthialu, D. Rex, A. Cannestra, J. Chen, and A. Toga, "Multiwavelength optical intrinsic signal imaging of cortical spreading depression," *J. Neurophysiol.* **88**, 2726–2735 (2002).
28. Y. Tomita, M. Tomita, I. Schiszler, T. Amano, N. Tanahashi, M. Kobari, H. Takeda, M. Ohtomo, and Y. Fukuuchi, "Repetitive concentric wave-ring spread of oligemia/hyperemia in the sensorimotor cortex accompanying K^+-induced spreading depression in rats and cats," *Neurosci. Lett.* **322**, 157–160 (2002).
29. P. Li, S. Chen, W. Luo, and Q. Luo, "*In vivo* optical imaging of intrinsic signal during cortical spreading depression in rats," *Prog. Biochem. Biophys.* **30**, 605–611 (2003).
30. P. Li, Q. Luo, W. Luo, S. Chen, H. Cheng, and S. Zeng, "Spatiotemporal characteristics of cerebral blood volume changes in rat somatosensory cortex evoked by sciatic nerve stimulation and obtained by optical imaging," *J. Biomed. Opt.* **8**(4), 629–635 (2003).
31. H. Nallet, E. T. MacKenzie, and S. Roussel, "Haemodynamic correlates of penumbral depolarization following focal cerebral ischaemia," *Brain Res.* **879**, 122–129 (2000).
32. G. Mies, "Blood flow dependent duration of cortical depolarizations in the periphery of focal ischemia of rat brain," *Neurosci. Lett.* **221**, 165–168 (1997).
33. P. Elisabeth, H. Nallet, E. T. MacKenzie, J. Seylaz, and S. Roussel, "Penumbral microcirculatory changes associated with peri-infarct depolarizations in the rat," *Stroke* **33**, 606–612 (2002).
34. L. H. Wang, S. L. Jacques, and L. Q. Zheng, "MCML—Monte Carlo modeling of photon transport in multi-layered tissues," *Comput. Methods Programs Biomed.* **47**, 131–146 (1995).
35. S. A. Prahl, "Optical absorption of hemoglobin," see http://omlc.ogi.edu/spectra/hemoglobin/ (1999).
36. A. N. Yarovslavsky, P. C. Schulze, I. V. Uaroslavsky, R. Schober, F. Ulrich, and H. J. Schwarzmaier, "Optical properties of selected native and coagulated human brain tissues in vitro in the visible and near infrared spectral range," *Phys. Med. Biol.* **47**, 2059–2063 (2002).
37. J. H. Choi, M. Wolf, V. Toronov, U. Wolf, C. Polzonetti, D. Hueber, L. P. Safonva, R. Gupta, A. Michalos, W. Mantulin, and E. Gratton, "Noninvasive determination of the optical properties of adult brain: near-infrared spectroscopy approach," *J. Biomed. Opt.* **9**(1), 221–229 (2004).